International Journal of Solids and Structures 49 (2012) 3233–3241

Contents lists available at SciVerse ScienceDirect

International Journal of Solids and Structures

journal homepage: www.elsevier.com/locate/ijsolstr

Theoretical modeling of guided wave propagation in a sandwich plate subjected to transient surface excitations

Sauvik Banerjee *, Chandrakant B. Pol [1]

Civil Engineering Department, Indian Institute of Technology Bombay, Powai, Mumbai 400 076, India

ARTICLE INFO

Article history:
Received 3 January 2012
Received in revised form 30 May 2012
Available online 31 July 2012

Keywords:
Sandwich structure
Global matrix method
Guided wave mode
Transient sources
Wavelet transformation

ABSTRACT

A fast and efficient two-dimensional (2D) semi-analytical model based on global matrix method is developed to study the general characteristics of guided wave propagation in a honeycomb composite sandwich structure (HCSS) subjected to time-dependent transient surface excitations. The HCSS used in this study has an extremely lightweight and thick nomex honeycomb core, which is sandwiched between two thin graphite woven composite skins. The homogenized material properties of the skin and the core are considered to be elastic and quasi-isotropic in nature. Far-field time history of surface displacements are calculated for vertical and horizontal tone-burst surface excitations that are representative of thickness and radial mode of vibrations of piezoelectric transducers, respectively. Results are compared with those obtained from Finite element modeling (FEM) in LS-DYNA showing good agreement. Wavelet transform is then performed on the time-domain signal to obtain the group velocities of the propagating modes for their accurate identification on the basis of the theoretical dispersion curve. It is found that the response signal is dominated by the first anti-symmetric mode for a vertical excitation, whereas, the signal characteristics are multimodal in nature with dominating higher order symmetric and anti-symmetric modes for a horizontal excitation. The model is expected to be helpful for appropriate guided wave mode tuning and rapid analysis of data for experimental detection of disbonds in these novel structures.
© 2012 Elsevier Ltd. All rights reserved.

1. Introduction

"Honeycomb composites" are sandwiched structures in which thin composite skins are bonded with adhesives to the two faces of extremely lightweight and relatively thick metallic honeycombs (Bitzer, 1997). Recently, these novel components are widely used in many modern applications, especially in aerospace and automotive industries with limited applications in civil infrastructure, such as highway bridges and building construction. The sandwich structures with honeycomb core exhibit unique and advantageous properties such as high strength-to-weight ratio and high energy-absorption capability, which make them very attractive for impact protection and mitigation related applications. Unfortunately, the bond between the honeycomb and the skin may degrade with age and service loads leading to separation of the load-bearing skin from the honeycomb (called "disbonds") and compromising the safety of the structure. To overcome the limitations of the conventional, costly, and time-consuming off-line non-destructive examination of large area structures, *in situ* inspection methods, which do not require the disassembly of the structure, have been subject of recent studies. Guided Lamb wave based methods offers such potential for detection of disbonds in sandwich structures (Hay et al., 2003; Diamanti et al., 2005; Baid et al., 2008). Tuning of appropriate guided wave modes plays an important role for non-destructive evaluation and health monitoring of composite structures using piezoelectric transducers (Maslov and Kundu, 1997; Xu and Giurgiutiu, 2007).

The general features of guided waves that can be transmitted in isotropic and anisotropic plates have been studied in great detail over the past several decades. Approximate thin-plate theories, such as, classical plate theory (C.P.T, under Kirchoff–Love kinematic assumption) and shear deformation plate theory (S.D.P.T) or Mindlin theory based on *a priori* ansatz on deformation were developed to obtain the analytical solution to a variety of problems involving the dynamic response of thin isotropic and anisotropic laminated plates (Achenbach, 1978; Nayfeh, 1995). The exact solution of three-dimensional guided wave problems consisting of multilayered, angle-ply laminates of finite thickness and large lateral dimensions subjected to various types of transient surface loads were presented in Lih and Mal (1996). A detailed discussion on the accuracy of approximate theories for wave field calculations in composite laminates in comparison to the exact theory was given in Lih and Mal (1995). It was shown that the C.P.T and

* Corresponding author. Tel.: +91 22 2576 7343; fax: +91 22 2576 7302.
E-mail addresses: sauvik@civil.iitb.ac.in (S. Banerjee), c_pol.civil@iitb.ac.in (C.B. Pol).
[1] Tel: +91 22 2576 7301; fax: +91 22 2576 7302.

0020-7683/$ - see front matter © 2012 Elsevier Ltd. All rights reserved.
http://dx.doi.org/10.1016/j.ijsolstr.2012.06.022

S.D.P.T produced desired results when the wavelength was much longer than the thickness of the plate, or in other words, the thickness-frequency product was very low. In contrast, theoretical models that can accurately capture the behavior of elastodynamic field due to high frequency transient sources in sandwich structures were not considered. Development of robust theoretical models is, of course, difficult because the dynamics of sandwich structures can be quite complicated with different behaviors in different regimes of frequency and wavelength.

In an early attempt, an analytical model for wave propagation in a three layered sandwiched structure with different boundary conditions was developed (Nilsson, 1990). The governing equations were derived partly by applying the general field equations (2-D theory) to the core and partly, by utilizing the thin plate/beam theory (1-D) to the laminates. The dispersion equation for the structure was derived and solved using the winding-integral technique. The other higher order models were also developed to study dynamic response of sandwich beams (Nosier et al., 1993; Backström and Nilsson, 2006; Sorokin, 2006; Qiao and Yang, 2007). However, these models used various *a priori* kinematic assumptions. A more efficient two-dimensional semi-analytical model based on the Thomson–Haskell method (Castaings and Hosten, 2003) has been developed for predicting the dispersion curves and the through-thickness, displacement, stress and energy flow distributions of guided modes propagating along sandwich plates made of anisotropic, viscoelastic material layers. The model is used to quantify the sensitivity of both the dispersion curves and the through-thickness mode shapes to the level of material viscoelasticity. Recently, a complete description of the dispersion relation with no restrictions on frequency and wavelength was provided for a sandwich structure comprising of isotropic layers (Liu and Bhattacharya, 2009). This is accomplished by transforming the wave equation to a Hamiltonian system and then using a transfer matrix approach for solving the Hamiltonian system. However, the above studies were only limited to frequency and wave-number domain and were not extended to the calculations of elastodynamic response due to transient sources.

In another variation, spectral finite element method (SFEM) based on first order laminated theory was used for wave propagation studies in laminated composite plate (Chakraborty and Gopalkrishnan, 2004). Commercially available finite element software, e.g., LS-DYNA, ABAQUS etc. have been used to solve impact and guided wave propagation problems in sandwich structures (Qiao and Yang, 2007; Song et al., 2009). Although the FEM can handle complex geometries and has the capability to accommodate reflections from the lateral boundaries, it is computationally much more intensive than the analytical methods discussed above.

In this article, a robust 2D semi-analytical model for rapid calculations of elastodynamic field due to transient sources on the surface of a laterally unbounded honeycomb-composite sandwich plate is presented. At the frequencies of interest here, the wavelengths are larger than the individual cell dimension of the honeycomb core, but can be shorter than the thickness of the core, so that homogenized material properties can be used for the core. The formulation is based on a global matrix method, where the displacements and stresses in each layer (skin or core) are 'exactly' represented in the frequency-wavenumber domain in terms of four unknown constants in each layer, which are then solved by applying the interface continuity conditions and the stress conditions on the free surfaces. Spatial and time domain solution is then obtained after performing a single wavenumber integral followed by frequency inversion using the fast Fourier transform. The surface motion is calculated for both vertical and horizontal narrowband excitations and compared with those obtained from finite element model in LS-DYNA (LSTC, 2007), for their mutual verification. In order to correctly identify the propagating modes, group velocities of these modes are calculated using wavelet transform (WT) of the calculated time-domain signal and compared with the theoretical group velocities showing good agreement.

2. Theoretical modeling

A global matrix method for the solution of wave propagation problems in multilayered anisotropic media subjected to time harmonic disturbances were presented in Mal (1988). In this article, the response problem was formulated using triple integral transforms involving one in time and two in space, leading to an exact representation of the elastodynamic field in the transformed frequency-wavenumber domain. The inversion of the transforms required numerical evaluation of a double wavenumber integral followed by frequency inversion using the fast Fourier transform (FFT) algorithm. An "adaptive surface-fitting scheme" using material dissipation was used in Lih and Mal (1996) to evaluate the double integral for dissipative media to achieve desired accuracy. In order to reduce the computational effort, a new integration scheme was proposed whereby the double integral is transformed, using contour integration, into a single integral, which is then evaluated numerically using conventional integration schemes (Banerjee et al., 2005). Unlike Thomson–Haskell method, which leads to numerical instabilities at higher frequencies (i.e. at higher wave numbers), the global matrix method presented in these articles doesn't suffer from such shortcomings.

The global matrix method is considered herein to develop a simplified 2D (plain-strain) semi-analytical model. The HCSS used in this study has an extremely lightweight and thick regular hexagonal honeycomb core (Hoo Fatt and Park, 2001), which is sandwiched between two 2/2 twill woven composite skins (Naik, 1994). The thicknesses of the composite skins and the honeycomb core are 1.78 mm. and 12.7 mm. respectively. The homogeneous material properties of the skins and the core are tabulated in Table 1. A schematic of the HCSS is shown in Fig. 1 along with the coordinate axes and a normal line load that are used for the problem formulation. Both the woven composite skins and the core exhibit transverse isotropy about the thickness direction (x_3). The required elastic constants for the 2D problem can be calculated using the information in Table 1 and are provided in Table 2 (Reddy 2003).

2.1. Matrix representation of the solution within a layer

For a 2D problem, the governing equations of motion in a layer of thickness H are given by:

$$\frac{\partial \sigma_{11}}{\partial x_1} + \frac{\partial \sigma_{13}}{\partial x_3} = \rho \frac{\partial^2 u_1}{\partial^2 t} \tag{1}$$

$$\frac{\partial \sigma_{13}}{\partial x_1} + \frac{\partial \sigma_{33}}{\partial x_3} = \rho \frac{\partial^2 u_3}{\partial^2 t} \tag{2}$$

Table 1
Material properties of the HCSS.

	E_1 (GPa)	E_2 (GPa)	E_3 (GPa)	G_{12} (GPa)	G_{13} (GPa)	G_{23} (GPa)	ν_{12}	ν_{13}	ν_{23}	ρ (g/cc)
Composite	48.7	48.7	11.6	18.5	4.2	4.2	0.32	0.27	0.27	1.42
Honeycomb	0.08040	0.08040	1.005	0.03220	0.1206	0.1206	0.25	0.02	0.02	0.064

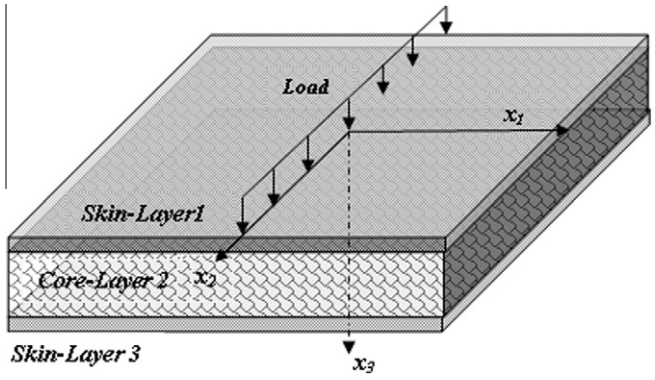

Fig. 1. Schematic representation of the honeycomb composite sandwich structure.

Table 2
Elastic material constants of the HCSS.

	c_{11} (GPa)	c_{13} (GPa)	c_{33} (GPa)	c_{55} (GPa)
Composite	56.1830	4.854	12.224	4.20
Honeycomb	0.0865	0.0272	1.0186	0.1206

The stress–strain relationships (Hooke's law) are stated as,

$$\begin{bmatrix}\sigma_{11}\\ \sigma_{33}\\ \sigma_{13}\end{bmatrix}=\begin{bmatrix}c_{11} & c_{13} & 0\\ c_{13} & c_{33} & 0\\ 0 & 0 & c_{55}\end{bmatrix}\begin{bmatrix}u_{1,1}\\ u_{3,3}\\ u_{1,3}+u_{3,1}\end{bmatrix} \tag{3}$$

We further assume that the potential functions are related to the displacement components through:

$$u_1=\frac{\partial\phi_1}{\partial x_1};\quad u_3=\frac{\partial\phi_3}{\partial x_3} \tag{4}$$

Substituting these displacement fields in the stress–strain relationships in Eq. (3), the governing equations of motion in terms of potential functions can be represented in matrix form:

$$\begin{bmatrix}c_{11}\frac{\partial^2}{\partial x_1^2}+c_{55}\frac{\partial^2}{\partial x_3^2}-\rho\frac{\partial^2}{\partial t^2} & (c_{13}+c_{55})\frac{\partial^2}{\partial x_3^2}\\ (c_{13}+c_{55})\frac{\partial^2}{\partial x_1^2} & c_{33}\frac{\partial^2}{\partial x_3^2}+c_{55}\frac{\partial^2}{\partial x_1^2}-\rho\frac{\partial^2}{\partial t^2}\end{bmatrix}\begin{bmatrix}\phi_1\\ \phi_3\end{bmatrix}=0 \tag{5}$$

We convert the field variables from spatial and time domain to the frequency and wavenumber domain by performing the following Fourier transformation:

$$\overline{\phi}(x_1,x_3,\omega)=\int_{-\infty}^{\infty}\phi(x_1,x_3,t)e^{-i\omega t}dt \tag{6}$$

and,

$$\hat{\phi}(\xi_1,\xi_3,\omega)=\int_{-\infty}^{\infty}\int_{-\infty}^{\infty}\bar{\phi}(x_1,x_3,\omega)e^{-i(\xi_1x+\xi_3x)}dx_1\,dx_3 \tag{7}$$

Applying Fourier transform on Eq. (5), the equations of motion in frequency and wavenumber domain can be written in matrix form as,

$$\begin{bmatrix}c_{11}\xi_1^2+c_{55}\xi_3^2-\rho\omega^2 & (c_{13}+c_{55})\xi_3^2\\ (c_{13}+c_{55})\xi_1^2 & c_{33}\xi_3^2+c_{55}\xi_1^2-\rho\omega^2\end{bmatrix}\begin{bmatrix}\hat{\phi}_1\\ \hat{\phi}_3\end{bmatrix}=0 \tag{8}$$

Solution to Eq.(8) is referred to as Eigen value problem. For a non trivial solution of the potential functions, the determinant of the 2×2 matrix has to be zero, which will give ξ_3^2 as roots (Eigen values) as a function of ξ_1. The characteristic equation is given by:

$$\underbrace{(a_1a_5)}_{A}\xi_3^4+\underbrace{\left[(a_5^2+a_1a_2-a_3^2)\xi_1^2-(a_1+a_5)\omega^2\right]}_{B}\xi_3^2+\underbrace{\left[(a_2\xi_1^2-\omega^2)(a_5\xi_1^2-\omega^2)\right]}_{C}=0 \tag{9}$$

which can be solved to obtain the two roots of ξ_3^2 as:

$$b_1=\frac{-B+\sqrt{B^2-4AC}}{2A}\quad\text{and}\quad b_2=\frac{-B-\sqrt{B^2-4AC}}{2A}$$

Thus, the roots of ξ_3 can be defined by the vertical wavenumbers , η_1, η_2. The "vertical" wavenumbers η_i ($i=1,2$) are subject to the restriction, $\mathrm{Im}(\eta_i)\geqslant0$, to ensure the outgoing wave condition at infinity and exponential decay of the evanescent waves in the layers at high frequencies. The next step is to reduce by one dimension the integrals in Eq. (7) using a contour in the complex ξ_3-plane consisting of the real axis together with a large semicircle in the upper half-plane, the contributions from this semicircle being vanishingly small (Buchwald, 1961). With this device, the integration with respect to ξ_3 can be replaced by appropriate contributions from the roots on the integrands.

Thus the general solution of the potential function can be written in matrix form as:

$$\begin{bmatrix}\hat{\phi}_1\\ \hat{\phi}_3\end{bmatrix}=\begin{bmatrix}q_{11} & q_{13}\\ q_{31} & q_{33}\end{bmatrix}\begin{bmatrix}e^{i\eta_1x_3} & 0\\ 0 & e^{i\eta_2x_3}\end{bmatrix}\begin{bmatrix}A_1^+\\ A_2^+\end{bmatrix}+\begin{bmatrix}q_{11} & q_{13}\\ q_{31} & q_{33}\end{bmatrix}\begin{bmatrix}e^{-i\eta_1x_3} & 0\\ 0 & e^{-i\eta_2x_3}\end{bmatrix}\begin{bmatrix}A_1^-\\ A_2^-\end{bmatrix} \tag{10}$$

Here, q_{ij} are the Eigen vectors and are given by:

$$q_{11}=b_1a_3,\quad q_{13}=b_2a_3,\quad q_{31}=\omega^2-a_2\xi_1^2-a_5b_1,\quad q_{33}=\omega^2-a_2\xi_1^2-a_5b_2$$

where, $a_1=\frac{c_{33}}{\rho}$, $a_2=\frac{c_{11}}{\rho}a_5=\frac{c_{55}}{\rho}$ and $a_3=\frac{(c_{13}+c_{55})}{\rho}$.

The quantities A_i^+ and A_i^- ($i=1,2$) are four unknown constants, which control the terms associated with upward and downward going waves as determined by the vertical wavenumbers η_i. It is therefore customary to express stresses and displacements in the frequency and wave number in condensed matrix form as:

$$\begin{bmatrix}\hat{u}_1\\ \hat{u}_3\\ \hat{\sigma}_{13}\\ \hat{\sigma}_{33}\end{bmatrix}=\begin{bmatrix}Q_{11} & Q_{12}\\ Q_{21} & Q_{22}\end{bmatrix}\begin{bmatrix}E_+(x_3) & 0\\ 0 & E_-(x_3)\end{bmatrix}\begin{bmatrix}A^+\\ A^-\end{bmatrix} \tag{11}$$

where,

$$Q_{11}=\begin{bmatrix}i\xi_1q_{11} & i\xi_1q_{13}\\ i\eta_1q_{31} & i\eta_2q_{33}\end{bmatrix},\quad Q_{12}=\begin{bmatrix}i\xi_1q_{11} & i\xi_1q_{13}\\ -i\eta_1q_{31} & -i\eta_2q_{33}\end{bmatrix}$$

$$Q_{21}=\begin{bmatrix}-c_{55}\eta_1\xi_1(q_{11}+q_{13}) & -c_{55}\eta_2\xi_1(q_{13}+q_{33})\\ -c_{13}\xi_1^2q_{11}-c_{33}\eta_1^2q_{31} & -c_{13}\xi_1^2q_{13}-c_{33}\eta_2^2q_{33}\end{bmatrix}$$

$$Q_{22}=\begin{bmatrix}c_{55}\eta_1\xi_1(q_{11}+q_{13}) & c_{55}\eta_2\xi_1(q_{13}+q_{33})\\ -c_{13}\xi_1^2q_{11}-c_{33}\eta_1^2q_{31} & -c_{13}\xi_1^2q_{13}-c_{33}\eta_2^2q_{33}\end{bmatrix}$$

$$\begin{bmatrix}A^+\\ A^-\end{bmatrix}=\begin{bmatrix}A_1^+\\ A_2^+\\ A_1^-\\ A_2^-\end{bmatrix}$$

$$E_+(x_3)=diag\begin{bmatrix}e^{i\eta_1x_3} & e^{i\eta_2x_3}\end{bmatrix}$$

$$E_-(x_3)=diag\begin{bmatrix}e^{i\eta_1(H-x_3)} & e^{i\eta_2(H-x_3)}\end{bmatrix}$$

The $E_+(x_3)$ wave signifies the down going wave while the $E_-(x_3)$ wave signifies the up wards going wave. The unknown constants must be solved from the imposed stress and displacement boundary conditions for a given problem at the top and bottom surfaces of the layer.

2.2. Global matrix formulation for the sandwich structure

In order to facilitate the application of the appropriate boundary conditions at the top and bottom surfaces and the interfaces, it is convenient to introduce the four-dimensional "stress-displacement vector : $\{\hat{S}^m\}$," in the transformed domain through

$$\left\{\hat{S}^m(\xi_1, x_3, \omega)\right\} = \left\{\hat{u}_i^m \;\; \hat{\sigma}_{i3}^m\right\} \quad (i = 1, 3) \tag{12}$$

where m denotes the layer number.

The arguments, ξ_1 and ω in $\{\hat{S}^m\}$ will be omitted for brevity. It should be noted that in absence of interfacial forces, $\{\hat{S}^m(x_3)\}$is continuous in the domain, $x_3^{m-1} < x < x_3^m$ and that in the mth layer, $\{\hat{S}^m(x_3)\}$ can be expressed in a partitioned matrix product form as

$$\{\hat{S}^m(x_3)\} = \begin{bmatrix} Q_{11}^m & Q_{12}^m \\ Q_{21}^m & Q_{22}^m \end{bmatrix} \begin{bmatrix} E_+^m(x_3) & 0 \\ 0 & E_-^m(x_3) \end{bmatrix} \begin{Bmatrix} A_+^m \\ A_-^m \end{Bmatrix} = [Q^m][E^m]\{A^m\} \tag{13}$$

where, $A_\pm^m$ are complex constants related to down going and up going waves within the mth layer, and $[E_\pm^m]$ are the 'vertical' propagation vectors:

$$\begin{aligned} [E_+^m(X_3)] &= Diag\left[e^{i\eta_1(X_3 - X_3^{m-1})} \quad e^{i\eta_2(X_3 - X_3^{m-1})}\right] \\ [E_-^m(X_3)] &= Diag\left[e^{i\eta_1(X_3^m - X_3)} \quad e^{i\eta_2(X_3^m - X_3)}\right] \end{aligned} \tag{14}$$

The $4m$ constants A^m must be determined from the interface conditions and the appropriate boundary conditions on the top and bottom surfaces of the plate.

In order to illustrate the solution procedure, we first consider the case where a time dependent normal point excitation is applied to the top surface of the plate denoted by $f(t)\delta(x_1 - 0)$ and its double Fourier transform by $\hat{f}(\omega)$. Thus the stress boundary conditions at the topmost surface and the lowermost free surface are given as,

$$[\hat{Q}^1][A^1] = [\hat{F}]; \quad \hat{Q}^3][A^3] = [0] \tag{15a)(15b}$$

where , $[\hat{Q}^1] = \begin{bmatrix} Q_{21}^1 & Q_{22}^1 E_-^1 \end{bmatrix}$; $[\hat{Q}^3] = \begin{bmatrix} Q_{21}^3 E_+^3 & Q_{22}^3 \end{bmatrix}$; $[\hat{F}] = \begin{bmatrix} \hat{\sigma}_{13} \\ \hat{\sigma}_{33} \end{bmatrix} = \begin{bmatrix} 0 \\ \hat{f} \end{bmatrix}$

In case of horizontal excitation, the force vector is given by:

$$[\hat{F}] = \begin{bmatrix} \hat{\sigma}_{13} \\ \hat{\sigma}_{33} \end{bmatrix} = \begin{bmatrix} \hat{f} \\ 0 \end{bmatrix} \tag{16}$$

If there are no disbonds at the two interfaces, the traction and displacement components must be continuous across the interfaces parallel to the X_1X_2-plane, which gives us:

$$\bar{u}_i^{(m)} = \bar{u}_i^{(m-1)}, \quad \bar{\sigma}_{i3}^{(m)} = \bar{\sigma}_{i3}^{(m-1)}, \quad X_3 = X_3^{m-1} \quad (\mathrm{m} = 2, 3)$$

where, X_3^{m-1} is the location of the interface between the layers m and m–1. Thus at the first interface i.e. of the layer 1 (skin) and 2 (core):

$$[Q^1][A^1] = [Q^2][A^2] \tag{17}$$

At the second interface i.e. of the layer 2 (core) and 3 (skin):

$$[Q'^2][A^2] = [Q^3][A^3] \tag{18}$$

where ,

$$[Q^1] = \begin{bmatrix} Q_{11}^1 E_+^1 & Q_{12}^1 \\ Q_{21}^1 E_+^1 & Q_{22}^1 \end{bmatrix}; \quad [Q^2] = \begin{bmatrix} Q_{11}^2 & Q_{12}^2 E_-^2 \\ Q_{21}^2 & Q_{22}^2 E_-^2 \end{bmatrix};$$
$$[Q'^2] = \begin{bmatrix} Q_{11}^2 E_+^2 & Q_{12}^2 \\ Q_{21}^2 E_+^2 & Q_{22}^2 \end{bmatrix}; \quad [Q^3] = \begin{bmatrix} Q_{11}^3 & Q_{12}^3 E_-^3 \\ Q_{21}^3 & Q_{22}^3 E_-^3 \end{bmatrix}$$

Finally, Eqs. 15(a,b), (17) and (18) can be represented in a condensed global matrix form as:

$$\begin{bmatrix} \hat{Q}^1 & 0 & 0 \\ Q^1 & -Q^2 & 0 \\ 0 & Q'^2 & -Q^3 \\ 0 & 0 & \hat{Q}^3 \end{bmatrix}_{12\times 12} \begin{bmatrix} A^1 \\ A^2 \\ A^3 \end{bmatrix}_{12\times 1} = \begin{bmatrix} \hat{F} \\ 0 \\ 0 \\ 0 \end{bmatrix}_{12\times 1} \tag{19}$$

The determinant of the 12×12 matrix will produce the desired dispersion relation of the form:

$$G(\xi_1, \omega) = 0 \tag{20}$$

For a range of values of ω, we can determine the roots as ξ_1 and subsequently determine the phase velocity c which is given by the relation $c = \omega/\xi_1$. The plot of the phase velocity 'c', versus the frequency ω gives the desired dispersion curve. The dispersion curve can be sought in terms of group velocity 'c_g', versus the frequency ω through $c_g = \frac{d\omega}{d\xi_1}$. Group velocity is often referred to as energy velocity as well. It should be noted that for a fixed frequency, infinite number of roots (real and complex) of ξ_1 can be obtained from Eq. (20). The real roots represent the propagating guided waves in the plate, while the complex roots represent non-propagating modes that decay exponentially with propagation distance from the source.

The unknown constants $[A]$ are determined using LU decomposition of Eq. (19). The vertical surface displacement can therefore be written in the following form:

$$\hat{u}_3 = \frac{F(\xi_1, \omega)}{G(\xi_1, \omega)} \tag{21}$$

It is now desired to invert the solution back to the spatial domain through:

$$\bar{u}_3(x_1, x_3, \omega) = \int_{-\infty}^{\infty} \frac{F(\xi_1, \omega)}{G(\xi_1, \omega)} e^{\iota\xi_1 x_1} d\xi_1 \tag{22}$$

The amplitudes of the non-propagating modes become negligible in comparison with the propagating modes at distances from the source larger than about only a few multiples of the plate thickness (Vasudevan and Mal, 1985). Since this condition is satisfied in most guided wave applications, the residue contributions from the complex roots can be ignored without significantly affecting the accuracy of the results. Thus, the integration in (22) can be solved exactly by applying Cauchy's residue theorem on the real roots of ξ_1 (ξ_r, where r = 1 to N, N = No. of real roots) as:

$$\bar{u}_3(x_1, x_3, \omega) = 2\pi i \sum_{r=1}^{N} \frac{F(\xi_r, \omega)}{\left.\frac{G(\xi_1, \omega)}{d\xi_1}\right|_{\xi_1 = \xi_r}} e^{i\xi_r x_1} \tag{23}$$

Finally, an inverse Fourier transform is performed to obtain the results in the time domain.

3. Results and discussions

3.1. Dispersion curves

Dispersion curves (frequency vs. group velocity) for the composite skin and the sandwich structure are presented in Fig. 2. As stated earlier, there exist multiple propagating wave modes that correspond to real roots of Eq. (20). Steepest descent method is used to extract these roots (Banerjee et al., 2005). The symmetric modes are designated S0, S1, S2, etc., while the anti-symmetric

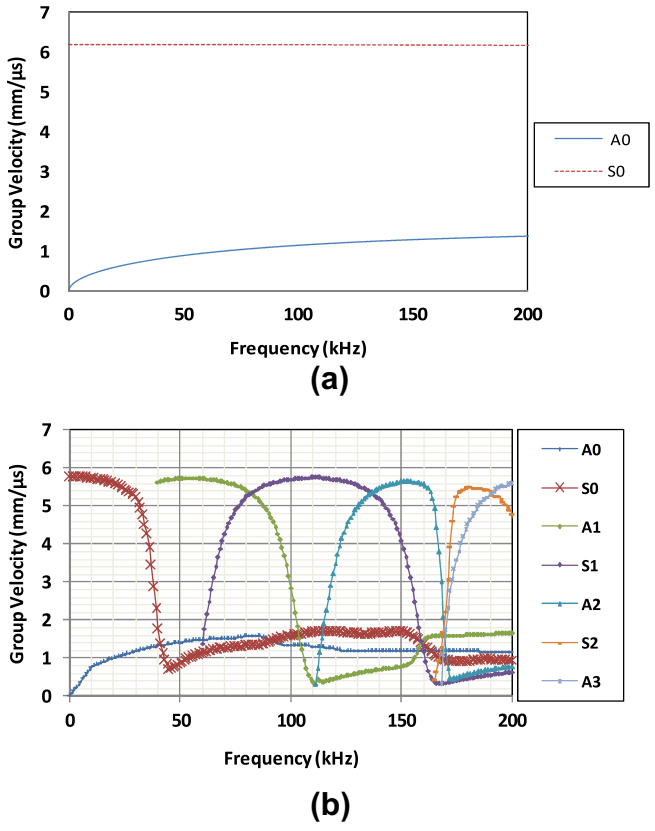

Fig. 2. Dispersion curve (frequency vs. group velocity) for (a) the composite skin and (b) the HCSS.

are designated A0, A1, A2, etc. (Achenbach, 1978). The dispersion curve for the skin, which is shown in Fig. 2(a), exhibits two possible wave modes, namely, first antisymmetric (A0) and first symmetric (S0) modes, for a wide frequency range. In contrary, the dispersion curve for the sandwich structure shown in Fig. 2(b) exhibits presence of higher order modes (e.g. second antisymmetric (A1), second symmetric (S1), and so on) after 50 kHz. The vast differences in the two dispersion curves are mainly governed by the differences in the thickness and the material properties of the respective plate. The effect of thickness may be explained in the context of well known Rayleigh-Lamb wave dispersion relations in isotropic plates (Achenbach, 1978). At low frequency-thickness (ωh) product, S0 mode is non-dispersive and A0 mode phase velocity varies as $\sqrt{\omega h}$. In the limit of high frequency-thickness (ωh), the phase velocity of both the S0 and A0 modes approach the Rayleigh wave speed (C_R), and all higher order modes approach the shear wave velocity (C_T), which is slightly higher than C_R. Thus, for the HCSS both the A0 and S0 modes quickly attain almost the same speed after only 50 kHz due to high ωh (approximately 0.8 MHz-mm at 50 kHz). This is, however, not the case for the plate comprising of skin alone since its ωh remains low (approximately 0.09 MHz-mm at 50 kHz). It should be further noted that the variations in the material properties of the skin and the core, and the thickness of the individual layer can affect the dispersion curve (Fig. 2(b)) for the HCSS. Nonetheless, the dispersion curve for the HCSS has the same structure as found earlier through experiments (Castaings and Hosten, 2003).

3.2. Response to surface loading

In order to understand the influence of modes on the guided wave propagation, surface displacements of the sandwich structure and the composite skin alone are calculated due to an excitation signal, which is a five cycle sine pulse in a Hanning window carrying a central frequency. This tone-burst signal is often deployed in nondestructive evaluation and health monitoring using PZT transducers because it produces a narrowband excitation that minimizes the effect of highly dispersive nature of guided wave modes. Two different excitation frequencies are considered: (a) 25 kHz and (b) 100 kHz. As per the dispersion curve for the HCSS, only two modes can possibly be excited at 25 kHz, whereas, more than two modes can appear for 100 kHz. A typical excitation signal at 100 kHz central frequency and its Fourier spectrum is shown in Fig. 3.

To examine the accuracy of the theoretical model, surface displacements are calculated at receiver distances both relatively closer (50 mm, roughly 3 times the total plate thickness) and far away (300 mm) from the source. 300 mm distance is chosen to allow adequate separation of propagating guided wave modes. The out-of-plane (u_3) surface displacement is calculated due to a vertical excitation (normal loading) to represent thickness mode of vibrations of piezoelectric transducers in an experiment, such that one of the transducers acts as a transmitter and the other one as a receiver. On the other hand, in-plane (u_1) surface displacement is calculated for a horizontal excitation (shear loading) representing radial mode of vibrations of piezoelectric transducers. The results are compared to those obtained from LS-DYNA simulations. In the LS-DYNA models, 4 noded plane-strain elements are used and the element size is controlled so that its dimension does not exceed one-tenth of the minimum wavelength, which is calculated based on the velocity of the slowest propagating mode at the excitation frequency. The skin and the core are discretized in 6 and 20 elements, respectively, along the thickness direction, and an element dimension of 0.5 mm is maintained along the x direction to meet the aforementioned condition in the frequency range of interest. Since the skin is thin, finer discretization is used in the thickness direction to capture the effect of shear deformation appropriately. The models are prepared long enough so that the edge reflections can be separated from the direct pass of the signal. A 4 m long model is prepared for the 25 kHz frequency excitation, and for the100 kHz frequency excitation, the model is 2 m lomg. A point force is applied at the mid node on the top surface and the displacements are calculated at a surface node to the right.

Theoretical and simulated responses for the 'composite skin alone' are compared in Figs. 4 and 5 for normal and horizontal excitations, respectively. Excellent agreements between the theoretical and simulated results are found for an excitation frequency of 100 kHz. Notably, for the normal excitation, the response is dominated by the A0 mode (Fig. 4), whereas, for the horizontal excitation, both A0 and S0 modes are present at 300 mm receiver distance and that the A0 mode is followed by a weak S0 mode (Fig. 5). Reflections form the edges are seen in Fig. 5. Since S0 mode has a group velocity of about 6 mm/μs at a frequency of 100 kHz, the first reflection at the receiver located at 50 mm (Fig. 5(a)) to the right of the source is expected to arrive at approximately 325 μs from the right edge. The second S0 mode reflection from the left edge of the model appears next.

The results for the 'HCSS' are presented in Figs. 6 and 7. In case of a normal excitation (Fig. 6), response is strongly influenced by the presence of A0 mode only at the two excitation frequencies (25 kHz and 100 kHz) and the receiver distances (50 mm and 300 mm). But, in case of a horizontal excitation (Fig. 7), the signal characteristics are multimodal in nature. At 25 kHz horizontal excitation (Fig. 7(a) and (b)), only two modes, A0 and S0, are present in the response signal. The separation between these two modes is evident for a receiver distance of 300 mm (Fig. 7(b)). But, at 100 kHz horizontal excitation (Fig. 7(c) and (d)), presence of dominating higher order symmetric and anti-symmetric modes

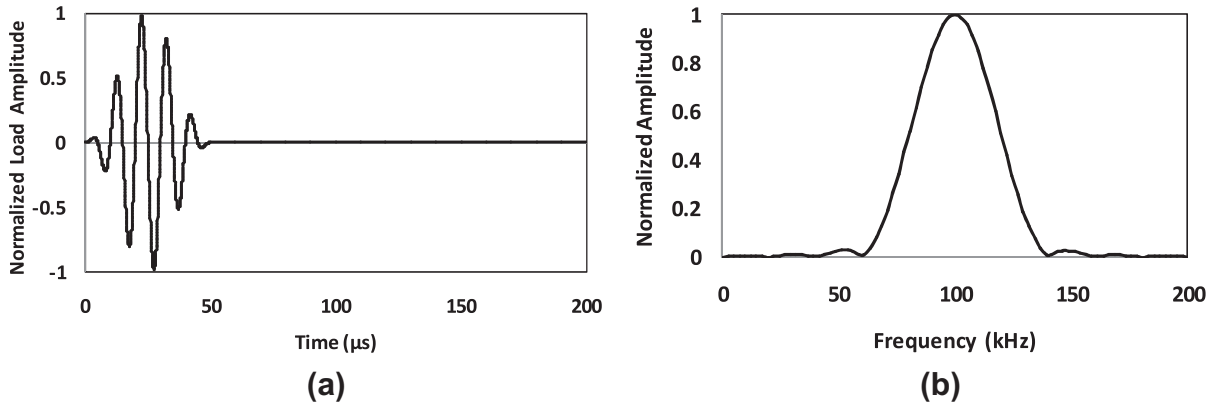

Fig. 3. (a) Excitation signal in the form of a five cycle sine pulse in a Hanning window carrying a central frequency at 100 kHz and (b) its Fourier spectrum.

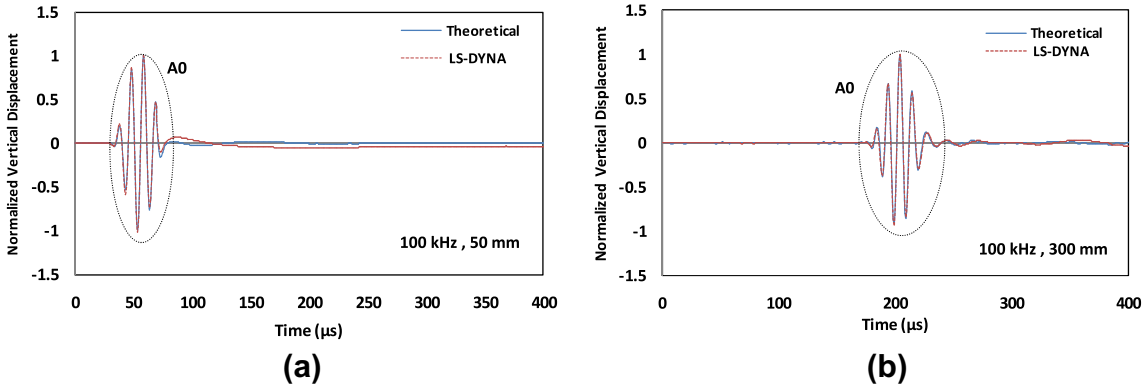

Fig. 4. Vertical surface displacement of the composite skin alone at a receiver distance of (a) 50 mm and (b) 300 mm, calculated from the theoretical model and the LSDYNA simulation for a normal excitation of 100 kHz.

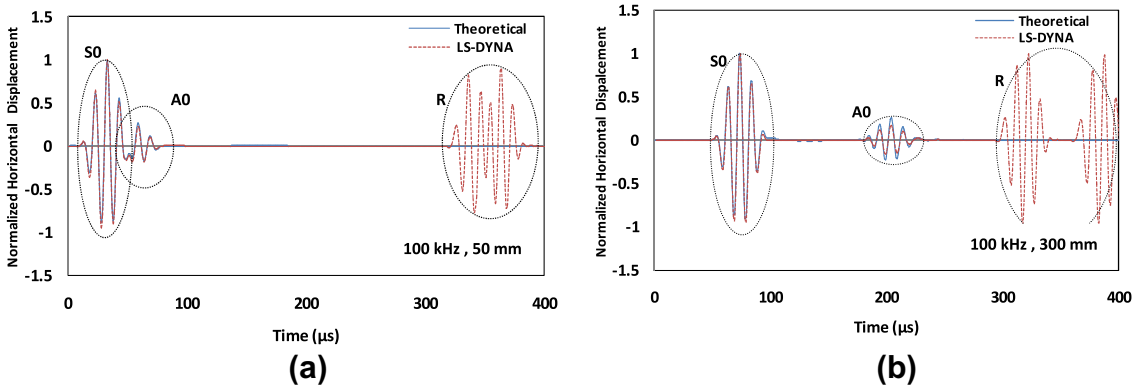

Fig. 5. Horizontal surface displacement of the composite skin alone at a receiver distance of (a) 50 mm and (b) 300 mm, calculated from the theoretical model and the LSDYNA simulation for a horizontal excitation of 100 kHz. Reflections from the edges are marked as R.

is observed. At a receiver distance of 50 mm (Fig. 7(c)), this effect cannot be visible, since not enough time is allowed for the propagating modes to separate as per their group velocities. Instead, this effect is prominent for a receiver distance of 300 mm (Fig. 7(d)). The approximate arrival time of the first reflected wave in Fig. 7(c) and (d) can be calculated based on the group velocity of the S1 mode at 100 kHz in a similar manner as the 'composite skin alone' case. It is, however, difficult to accurately identify the propagating modes from the time domain signal because their arrival timings are not clear. Therefore, wavelet transformation technique is used for accurate estimation of group velocities of the propagating modes in the response signal for their appropriate identification.

3.3. Wavelet transformation for identification of modes

Wavelet transformation (WT) is a powerful tool of time–frequency analyses for sudden change in signal, accompanying energy reflection, transmission, and mode conversion. The major advantage of WT is that it retains both the time and frequency domain information of the raw time domain data, thereby, enabling estimation of time of arrival of propagating modes in a wave packet

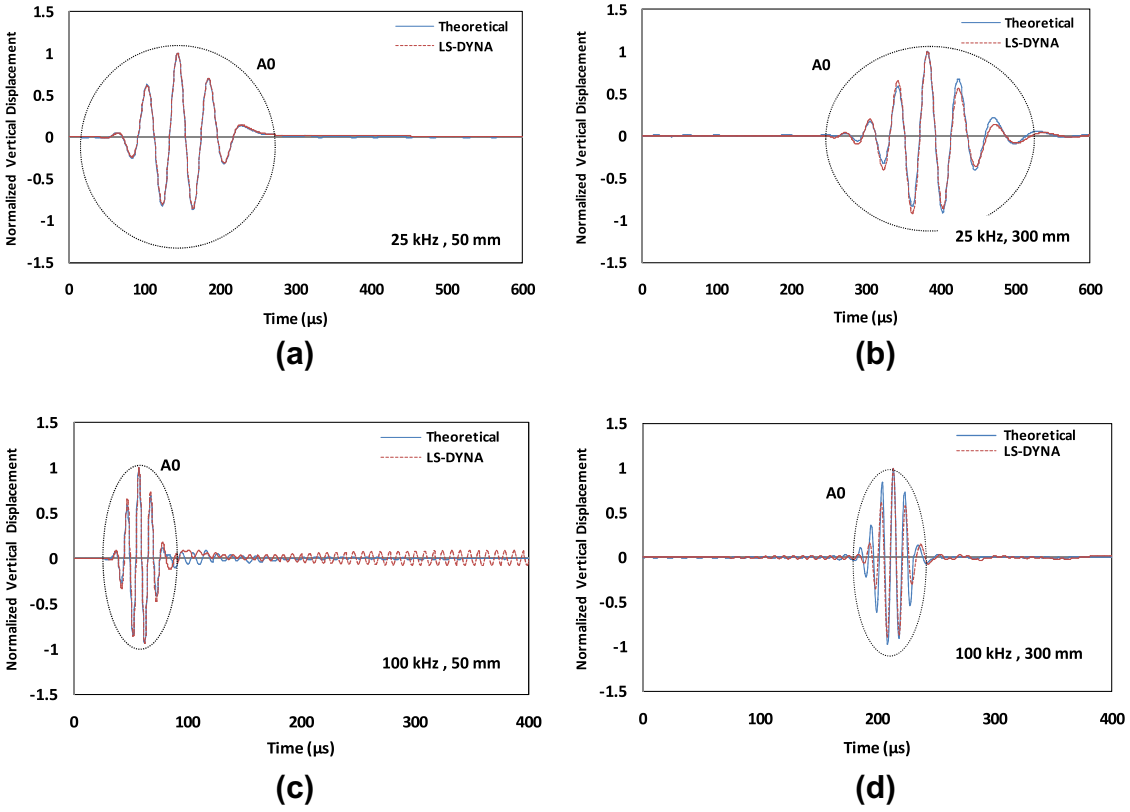

Fig. 6. Vertical surface displacements of the HCSS at 50 mm and 300 mm receiver distances calculated from the theoretical model and the LSDYNA simulation for a normal excitation of (a,b) 25 kHz and (c,d) 100 kHz.

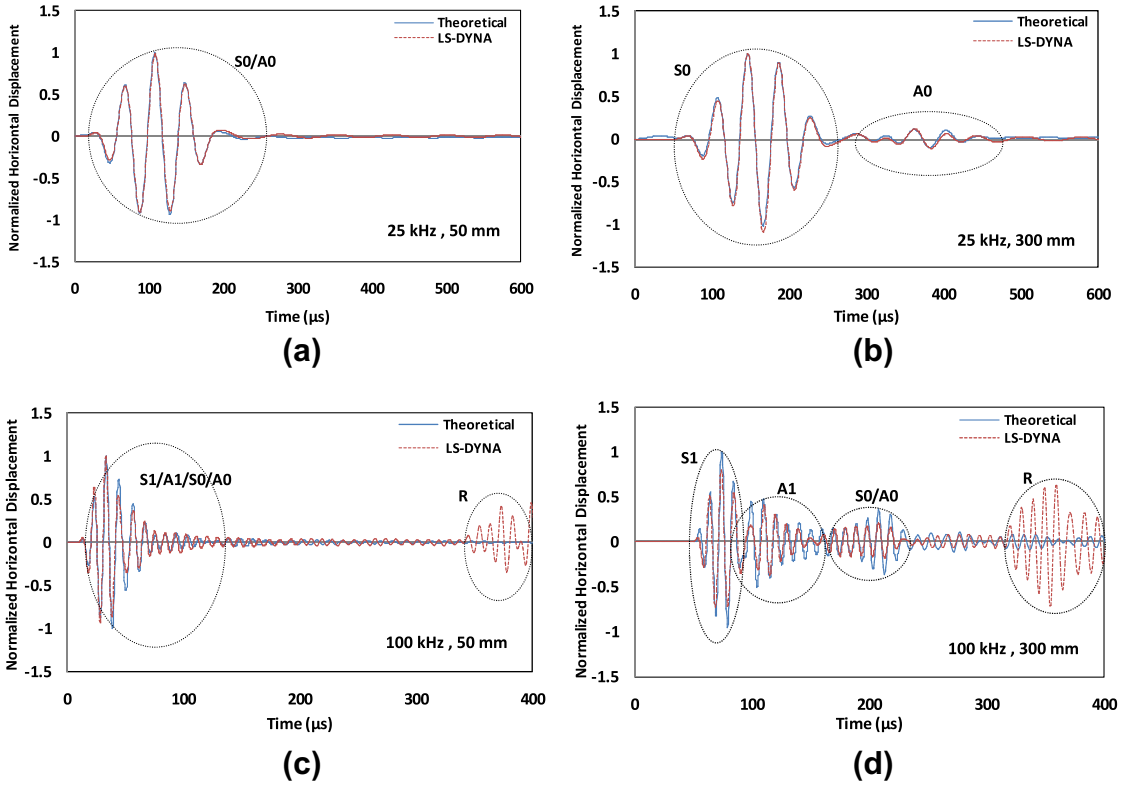

Fig. 7. Horizontal surface displacements of the HCSS at 50 mm and 300 mm receiver distances calculated from the theoretical model and the LSDYNA simulation for a horizontal excitation of (a,b) 25 kHz and (c,d) 100 kHz. Reflections from the edges are marked as R.

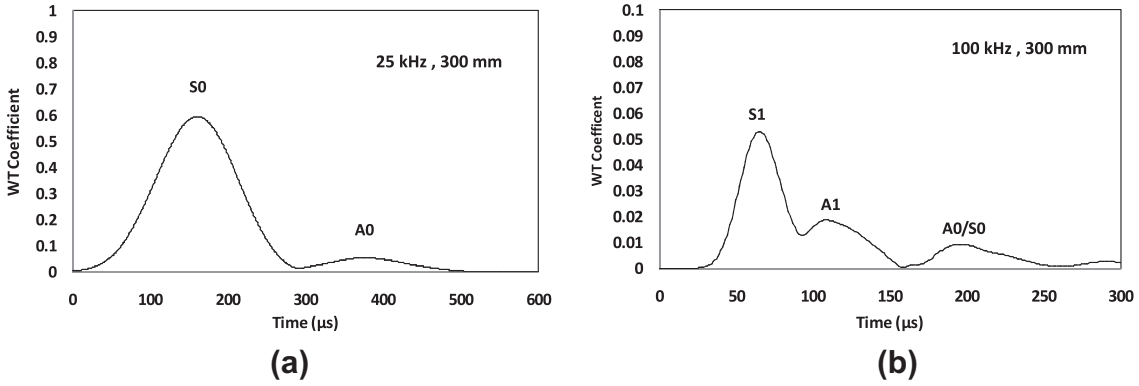

Fig. 8. WTC profile of the response signal at a distance of 300 mm for (a) 25 kHz and (b) 100 kHz horizontal excitation.

at a particular excitation frequency. All the wavelet transformations (WTs) are calculated with AGU-Vallen Wavelet that uses a Gabor function as the mother wavelet with a central frequency of 7 MHz, and has been used extensively in the pioneering research of wavelet analysis in the field of guided wave acoustic emission (Hamstad et al., 2002). Group velocity is usually considered to be propagation speed of a wave packet (envelope) with a central frequency carrying maximum energy, whereas, individual frequency component in the packet is propagated at its phase velocity. Thus, it is convenient to use wavelet transformed data of the source and the received signal for the calculation of group velocity of a propagating mode as follows:

$$c_g = \frac{d}{\Delta t} \tag{22}$$

where, d is distance between the source (excitaion) and the receiver, and Δt is defined as the time interval between the peaks of the WT envelopes of the source signal and the propagating mode in the received signal, respectively, at the central frequency.

The wavelet transform coefficient (WTC) profiles of the response signals at a distance of 300 mm for 25 kHz and 100 kHz horizontal excitations are presented in Fig. 8(a) and (b), respectively. As expected from the dispersion curve, S1 mode is faster than the A1 mode at an excitation frequency of 100 kHz, however, A1 mode is highly dispersive in the associated frequency bandwidth of the excitation. This behavior is just reversed if an excitation frequency of 75 kHz is considered as shown in Fig. 9. In this case S1 mode is slower than the A1 mode and exhibits dispersive nature. It should be noted that it is difficult to separate A0 and S0 modes at higher frequencies (e. g 75 kHz and 100 kHz), since their group velocities do not differ much and that the amplitudes of these two modes are also small compared to higher order modes. The group velocities calculated using the WT technique (Eq. (22)) and the theoretical model are compared in Table 3, showing good agreement. Since WT coefficients are indirectly related to the signal strength, relative magnitudes between the WTC peaks for the two different wave modes indicate relative difference in the strength of the modes. It is further observed that the magnitudes of WTC are gradually decreasing with the increasing frequency. This indicates that the signal strength is reduced at the high frequency excitation signal when compared to the low frequency excitation signal. It is due to the fact that the time-band-

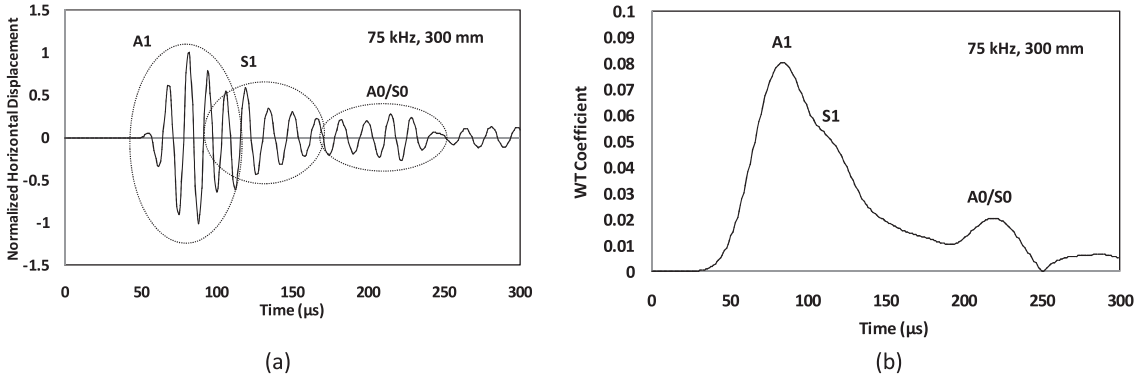

Fig. 9. (a) The response signal and (b) its WTC profile at a distance of 300 mm for 75 kHz horizontal excitation.

Table 3
The group velocities for various modes calculated using the WT technique and the theoretical model.

Frequency (kHz)	Theoretical group velocity (mm/μs)				WT group velocity (mm/μs)			
	A1	S1	A0	S0	A1	S1	A0	S0
25	Absent	Absent	1.10	5.45	Absent	Absent	1.08	5.41
75	5.62	4.26	1.51	1.27	5.61	4.21	–	–
100	2.84	5.71	1.35	1.59	2.86	5.78	–	–

width of the input signal is reduced at a high frequency while its peak amplitude remains unchanged in comparison to the low frequency excitation signal.

4. Conclusions

A 2D semi-analytical model with no prior restrictions on frequency and wavelength is presented in an effort to understand multimodal characteristics of propagating guided waves (GW) in HCSS due to transient sources. The wavenumber integral technique, however, takes into account contributions from only propagating GW modes (real roots of dispersion equation). This enables rapid calculation of 'far-field' surface motion in HCSS with a good accuracy when compared to LS-DYNA simulation results. While execution of LSDYNA model takes more than an hour, theoretical model takes only a few second. In HCSS, for all cases of normal loadings, response is strongly influenced by the presence of A0 mode. In contrary, the surface motion is dominated by S0 mode followed by a weak A0 mode at a low frequency horizontal excitation, whereas, the presence of higher order modes (e.g. S1, A1) is seen to dominate the surface motion at a high frequency horizontal excitation . For the HCSS, it is noticed that at the 100 kHz frequency, the wavelength of the A0 mode is roughly 10 mm, which is less than the thickness of the plate as well as that of the core. Thus, it is evident that the approximate theories, in principle, cannot even realistically model A0 mode at this frequency. For the 'skin alone', however, approximate theories can be used in the frequency range of interest since the wavelength is much longer than the thickness of the plate (Banerjee et al., 2004). The wavelet transformation technique is used as a potential tool to identify the propagating guided wave modes accurately on the basis of theoretical dispersion curve. The semi-analytical model is expected to help in the selection and tuning of appropriate guided wave modes for efficient damage detection in sandwich structures using PZT transducers. Another major advantage of the model is that the integration scheme can be exploited to obtain the time-domain solution for any specific propagating mode. In addition, it is possible to introduce dissipative material characteristics in the model by using complex elastic modulii, however, full integration of Eq. (22) should be performed that can increase the computational cost manifold.

Acknowledgments

This research was supported by Indian Space Research Organization under Grant No. 11ISROC001. The authors wish to thank Prof. Ajit Mal, Mechanical and Aerospace Engineering Department, University of California Los Angeles for his helpful suggestions during the course of this research.

References

Achenbach, J.D., 1978. Wave Propagation in Elastic Solids. North-Holland, New York.
Backström, D., Nilsson, A., 2006. Modeling flexural vibration of a sandwich beam using modified fourth-order theory. J. Sandwich Struct. Mater. 8, 465–476.
Baid, H., Banerjee, S., Mal, A.K., Joshi, S., 2008. Detection of disbonds in a honeycomb composite structure using guided waves. In: Proceedings of SPIE, Smart Structures and Materials & Nondestructive Evaluation and Health Monitoring VI, March 9–13, San Deigo, California.
Banerjee, S., Mal, A.K., Prosser, W.H., 2004. Analysis of transient Lamb waves generated by dynamic surface sources in thin composite plates. J. Acoust. Soc. Am. 115 (5), 1905–1911.
Banerjee, S., Prosser, W.H., Mal, A.K., 2005. Calculation of the response of a composite plate to localized dynamic surface loads using a new wave number integral method. ASME J. Appl. Mech. 72, 18–24.
Bitzer, T., 1997. Honeycomb Technology: Materials, Design, Manufacturing, Applications and Testing. Chapman & Hall, London.
Buchwald, V.T., 1961. Rayleigh waves in transversely isotropic media. Quart. J. Mech. Appl. Math. XIV, 293–317.
Castaings, M., Hosten, B., 2003. Guided waves propagating in sandwich structures made of anisotropic, viscoelastic, composite materials. J. Acoust. Soc. Am. 113, 2622–2634.
Chakraborty, A., Gopalkrishnan, S., 2004. A spectrally formulated finite element for wave propagation analysis in laminated composite media. Int. J. Solids Struct. 41, 5155–5183.
Diamanti, K., Soutis, C., Hodgkinson, J.M., 2005. A lamb waves for the non-destructive inspection of monolithic and sandwich composite beams. Compos. Part A 36, 189–195.
Hamstad, M.A., O'Gallaghar, A., Gary, J., 2002. A wavelet transformation applied to acoustic emission signals: part 1: source identification. J. Acoustic Emission 20, 39–61.
Hay, T.R., Wei, L., Rose, J.L., 2003. Rapid inspection of composite skin–honeycomb core structures with ultrasonic guided waves. J. Compos. Mater. 37, 929–939.
Hoo Fatt, M.S., Park, K.S., 2001. Dynamic models for low velocity impact damage of composite sandwich panels – part a: deformation. Compos. Struct. 52, 335–351.
Lih, S.S., Mal, A.K., 1995. On the accuracy of approximate plate theories for wave field calculations in composite laminates. Wave Motion 21, 17–34.
Lih, S.S., Mal, A.K., 1996. Response of multilayered composite laminates to dynamic surface loads. Compos. Part B 27B, 633–641.
Liu, L.P., Bhattacharya, K., 2009. Wave propagation in a sandwich structure. Int. J. Solids Struct. 46, 3290–3300.
LSTC, 2007. LS-DYNA Keyword User's Manual, Volume 1, Version 971, Livermore Software Technology Corporation (LSTC).
Mal, A.K., 1988. Wave propagation in layered composite laminates under periodic surface loads. Wave Motion 10, 257–266.
Maslov, K.I., Kundu, T., 1997. Selection of lamb modes for detecting internal defects in laminated composites. Ultrasonics 35, 141–150.
Naik, N.K., 1994. Woven Fabric Composites. Technomic Publishing Co., Inc., Lancaster, PA.
Nayfeh, A.H., 1995. Wave propagation in layered anisotropic media with applications to composites. In: Achenbach, J.D. (Ed.), North-Holland Series in Applied Mathematics and Mechanics, vol. 39. Elsevier Science, Amsterdam.
Nilsson, A.C., 1990. Wave propagation in and sound transmission through sandwich plates. J. Sound Vib. 138, 73–94.
Nosier, A., Kapania, R.K., Reddy, J.N., 1993. Free vibration analysis of laminated plates using a layer-wise theory. AIAA J. 31, 2335–2346.
Qiao, P., Yang, M., 2007. Impact analysis of fiber reinforced polymer honeycomb composite sandwich beams. Compos. Part B 38 (739–750), 2007.
Reddy, J.N., 2003. Mechanics of Laminated Composite Plates and Shells: Theory and Analysis, second ed. CRC Press.
Song, F., Huang, G.L., Hudson, K., 2009. Guided wave propagation in honeycomb sandwich structures using a piezoelectric actuator/sensor system. Smart Mater. Struct. 18, 125007.
Sorokin, S.V., 2006. Analysis of propagation of waves of purely shear deformation in a sandwich plate. J. Sound Vib. 291, 1208–1220.
Vasudevan, N., Mal, A.K., 1985. Response of an elastic plate to localized transient sources. ASME J. Appl. Mech. 107, 356–362.
Xu, B., Giurgiutiu, V., 2007. Single mode tuning effects on Lamb wave time reversal with piezoelectric wafer active sensors for structural health monitoring. J. Nondestruct. Eval. 26, 123–134.